VPS VIBRATIONS IN PHYSICAL SYSTEMS

DOI: 10.21008/j.0860-6897.2024.3.14
Vibrations in Physical Systems, 2024, 35(3), 2024314

Theoretical and numerical studies of low-frequency reverberant sound field in coupled rooms

Mirosław MEISSNER

Institute of Fundamental Technological Research, Polish Academy of Sciences, Pawińskiego 5B, 02-106 Warsaw

Corresponding author: Mirosław MEISSNER, email: mmeissn@ippt.pan.pl

Abstract The paper examines the low-frequency reverberation sound field in coupled-room systems. In theoretical model, the modal expansion of sound pressure was applied, while in numerical procedure, the discrete Hilbert transform was used to determine the amplitude of decaying sound. Computer simulations were performed for a room system consisting of two connected rectangular rooms. Eigenfunctions and eigenfrequencies of this system were determined by the finite element method. Simulation results showed that for the hard-walled room system the sound decay is almost exponential for frequencies of modes localized in one of the subrooms. Acoustical treatment of the ceiling significantly reduced reverberation. However, due to beating effects and modal overlap, a large irregularity of sound decay curves has occurred. This makes it difficult to correctly qualify the sound decay, because in this case it is practically impossible to characterize the reverberation process with only one or at most two decay times.

Keywords: room acoustics, coupled rooms, reverberant sound field, mode localization, sound decay.

1. Introduction

Acoustical properties of coupled rooms are of great interest in the context of architectural acoustics, since coupled-volume systems, composed of two or more spaces that are connected through acoustically transparent openings, can be found in various buildings and constructions. Examples are architectural objects such as churches with naves and side galleries, theatres with stage houses, concert halls fitted with reverberation chambers, the orchestra pit and balconies in opera houses, and irregularly shaped rooms such as L- and T-shaped enclosures. Nowadays, many numerical methods can be used to estimate the sound field in coupled rooms, like diffusion-equation models [1, 2], statistical-acoustic models [3, 4], the geometrical acoustics [5, 6] and the modal expansion method [7], also known as the eigenmode analysis. The geometrical acoustics applies at best to rooms with dimensions large compared to the wavelength. This method neglects diffraction phenomena since a propagation in straight lines is its main postulate, therefore, the results obtained with such method are inaccurate for coupled rooms and enclosures with complex shapes. The modal expansion method is a technique used for vibration analysis of mechanical objects and structures, thus, it has been applied in several branches of technical sciences. In room acoustics, this method yields the resonant modes of pressure vibrations, and the sound field is expressed as a linear combination of the resonant modes. The modal expansion method is more difficult to apply for coupled rooms and irregularly shaped enclosures, but it fully describes a wave nature of the sound field as well as creation of vortices in the active intensity vector field [8]. The modal expansion approach can be applied in a low-frequency range, so this method is especially useful to the room systems with dimensions comparable with the sound wavelength.

In the low-frequency range, the coupled-room systems exhibit some interesting effects like: the mode degeneration due to modification of the coupling area, confinement of an acoustic energy in a part of room system, called the mode localization, and a considerable difference between a rate of sound decay in early and late stages of the reverberant process, known as a double sloped decay. These phenomena have been investigated by the author in the papers [9-11]. The current work focuses on theoretical and numerical predictions of a spatial distribution of the low-frequency reverberant sound field in coupled rooms. The research explores the geometry that often occurs in the reality when two rectangular subrooms with the same heights are connected to one another. A response of the room system to the sound excitation is described by means of a modal expansion of the sound pressure for a lightly damped room system with complex-valued boundary conditions on walls. Eigenfunctions and eigenfrequencies for this room system were calculated using the finite element method.

2. Theoretical analysis

2.1. Low-frequency room acoustics

In the low-frequency range, a theoretical method most suitable for modeling a sound field in coupled rooms is the modal expansion method. In this method, the sound pressure $p(\mathbf{r},t)$ in the field point $\mathbf{r}=(x,y,z)$ is a superposition of responses of acoustic modes excited by a source, so it can be given by

$$p(\mathbf{r},t)=\sum_{m=1}^{\infty}p_m(t)\Phi_m(\mathbf{r}), \tag{1}$$

where p_m are time-dependent modal amplitudes, Φ_m are eigenfunctions and each of them is related to the corresponding eigenfrequency ω_m. Since the theoretical model is dedicated to lightly damped rooms, the eigenfunctions Φ_m can be approximated by real-valued eigenfunctions determined for the rigid boundary surfaces. It should be noted that analytical forms of eigenfunctions Φ_m are known only for the simplest geometry such as a cuboid or cylinder, so for irregularly shaped enclosures such as coupled-room systems, the determination of eigenfunctions Φ_m will require the use of numerical methods.

The procedure for finding modal amplitudes p_m was presented in [7], and it can be shown that for lightly damped room systems, the amplitude p_m is a solution of the following equation:

$$\frac{\partial^2 p_m}{\partial t^2}+2\xi_m\frac{\partial p_m}{\partial t}+\omega_m^2 p_m=c^2\int_V q(\mathbf{r},t)\Phi_m(\mathbf{r})\mathrm{d}V=s_m(t), \tag{2}$$

where c is the sound speed, $q(\mathbf{r},t)$ is the volume sound source, $s_m(t)$ is a modal source function, V is the volume of a room system and the coefficients ξ_m are determined by

$$\xi_m=r_m+\mathrm{j}\varphi_m=\frac{c}{2}\int_S\frac{\Phi_m^2(\mathbf{r}_s)}{\zeta}\mathrm{d}S, \tag{3}$$

where ζ is the complex impedance on the wall surface S, normalized by ρc, ρ is the air density, $\mathbf{r}_s$ is a position coordinate on the surface S and $\mathrm{j}=\sqrt{-1}$. In order to solve Eq. (2), the method of variation of parameters was employed [12]. Using this method the general solution of Eq. (2) was found as

$$\begin{aligned}p_m(t)=&\frac{[x_m(t)y_m'(t_0)-y_m(t)x_m'(t_0)]p_m(t_0)}{W_m(t_0)}-\frac{[x_m(t)y_m(t_0)-y_m(t)x_m(t_0)]p_m'(t_0)}{W_m(t_0)}\\&-x_m(t)\int_{t_0}^{t}\frac{s_m(\tau)y_m(\tau)}{W_m(\tau)}\mathrm{d}\tau+y_m(t)\int_{t_0}^{t}\frac{s_m(\tau)x_m(\tau)}{W_m(\tau)}\mathrm{d}\tau,\end{aligned} \tag{4}$$

where the functions $x_m(t)$ and $y_m(t)$ having the following forms:

$$x_m(t)=e^{-(\xi_m+\mathrm{j}\psi_m)t},\quad y_m(t)=e^{-(\xi_m-\mathrm{j}\psi_m)t} \tag{5a, b}$$

represent a fundamental set of solutions of homogeneous differential equations

$$\frac{\partial^2 p_m}{\partial t^2}+2\xi_m\frac{\partial p_m}{\partial t}+\omega_m^2 p_m=0, \tag{6}$$

the function $W_m(t)=x_m(t)y_m'(t)-y_m(t)x_m'(t)$ is the Wronskian of $x_m(t)$ and $y_m(t)$, $p_m(t_0)$ and $p_m'(t_0)$ are the initial conditions, and ψ_m is the complex frequency for the mth mode

$$\psi_m=\Omega_m+\mathrm{j}\vartheta_m=\sqrt{\frac{a_m+\sqrt{a_m^2+b_m^2}}{2}}+\mathrm{j}\sqrt{\frac{-a_m+\sqrt{a_m^2+b_m^2}}{2}}, \tag{7}$$

where $a_m=\omega_m^2-r_m^2+\varphi_m^2$ and $b_m=-2r_m\varphi_m$. Inserting the functions $x_m(t)$ and $y_m(t)$ in Eq. (4) and making some mathematical transformations one can get

$$\begin{aligned}p_m(t)=&\frac{e^{-\xi_m t}}{2\mathrm{j}\psi_m}\left[e^{\mathrm{j}\psi_m t}\int_{t_0}^{t}s_m(\tau)e^{(\xi_m-\mathrm{j}\psi_m)\tau}\mathrm{d}\tau-e^{-\mathrm{j}\psi_m t}\int_{t_0}^{t}s_m(\tau)e^{(\xi_m+\mathrm{j}\psi_m)\tau}\mathrm{d}\tau\right]\\&+e^{-\xi_m(t-t_0)}\left\{p_m(t_0)\cos[\psi_m(t-t_0)]+\frac{\xi_m p_m(t_0)+p_m'(t_0)}{\psi_m}\sin[\psi_m(t-t_0)]\right\}.\end{aligned} \tag{8}$$

The first component on the right-hand side of Eq. (8) describes a modal response of a room system to the sound excitation defined by the modal source function $s_m(t)$. Therefore, using this component it is possible to analyze low-frequency transients or, in the case of a pure-tone sound source, to study the sound build-up and the formation of a steady state. The second component on the right-hand side of Eq. (8) describes the decay of modal amplitudes when the sound source is turned off, so the modal sound field after this moment is determined only by the initial conditions $p_m(t_0)$ and $p'_m(t_0)$. It is worth emphasizing that in room acoustics it is of particular importance to predict the reverberant sound field after switching off a pure-tone excitation.

2.2. Reverberant sound field

When in a coupled-room system there is a pure-tone sound source, which operates with constant power, energy losses on absorbing boundary surfaces are covered by the source and in the steady-state, which is usually reached during short time after a source start, the absorptive power is equal to that produced by the source. If the sound source is switched off, the acoustic energy accumulated inside a room system is dissipated on boundary surfaces and a reverberant sound field appears due to the common decay of acoustic modes. In order to simplify the analysis, it is assumed that the source stops at the time $t_0 = 0$, hence using Eq. (8) one can obtain the following expression describing a decay of the *m*th mode:

$$p_m(t) = e^{-\xi_m t}\left[p_m(0)\cos(\psi_m t) + \frac{\xi_m p_m(0) + p'_m(0)}{\psi_m}\sin(\psi_m t)\right]. \tag{9}$$

In Eq. (9) the initial conditions $p_m(0)$ and $p'_m(0)$ represent the modal amplitude and its time derivate when a steady-state in a room system is reached. From theoretical point of view, a steady-state is achieved when a time interval between the current time t and a moment of starting a pure-tone source is infinitely long. Thus, in Eq. (8) it must be assumed that $t_0 = -\infty$. Because in this case the initial conditions $p_m(t_0) = p'_m(t_0) = 0$ are met, the formula for a steady-state modal behavior takes the following form

$$p_m(t) = \frac{e^{-\xi_m t}}{2\mathrm{j}\psi_m}\left[e^{\mathrm{j}\psi_m t}\int_{-\infty}^{t} s_m(\tau)e^{(\xi_m - \mathrm{j}\psi_m)\tau}\mathrm{d}\tau - e^{-\mathrm{j}\psi_m t}\int_{-\infty}^{t} s_m(\tau)e^{(\xi_m + \mathrm{j}\psi_m)\tau}\mathrm{d}\tau\right]. \tag{10}$$

If the sound source is located at the point $\mathbf{r}_0 = (x_0, y_0, z_0)$ and ω is the source angular frequency, the volume sound source $q(\mathbf{r}, t)$ in Eq. (2) has the form:

$$q(\mathbf{r}, t) = Q\delta(\mathbf{r} - \mathbf{r}_0)e^{\mathrm{j}\omega t}, \tag{11}$$

where the factor Q depends on the source power W according to the formula $Q = \sqrt{8\pi\rho c W}$ [13], therefore for this source the modal source function $s_m(t)$ can be determined from the following equation:

$$s_m(t) = Qc^2\Phi_m(\mathbf{r}_0)e^{\mathrm{j}\omega t}. \tag{12}$$

After inserting Eq. (12) into Eq. (10), the conditions $p_m(0)$ and $p'_m(0)$ for a steady-state can be found as

$$p_m(0) = \frac{Qc^2\Phi_m(\mathbf{r}_0)}{\omega_m^2 - \omega^2 + 2\mathrm{j}\omega\xi_m}, \tag{13}$$

$$p'_m(0) = \mathrm{j}\omega p_m(0), \tag{14}$$

where the identity $\omega_m^2 = \xi_m^2 + \psi_m^2$ was applied. Finally, substituting these conditions into Eq. (9) and using the obtained result in Eq. (1) yield the following equation:

$$p(\mathbf{r}, t) = Qc^2\sum_{m=1}^{\infty}\frac{e^{-\xi_m t}\Phi_m(\mathbf{r}_0)\Phi_m(\mathbf{r})}{\omega_m^2 - \omega^2 + 2\mathrm{j}\omega\xi_m}\left[\cos(\psi_m t) + \frac{(\xi_m + \mathrm{j}\omega)\sin(\psi_m t)}{\psi_m}\right] \tag{15}$$

describing a decay of the indoor sound pressure after switching off the pure-tone source. Equation (15) enables one to determine various properties of the reverberant sound field. Firstly, using Eq. (15) it is possible to predict changes in a spatial distribution of the pressure amplitude with increasing time, and secondly, at a given position $\mathbf{r}$ of the field point, this equation allows to determine the temporal changes in the pressure amplitude and then estimate the reverberation time.

As follows from Eq. (15), the reverberant sound is a superposition of decaying modal vibrations, which means that the pressure amplitude is time-dependent. Therefore, this amplitude is best calculated using the discrete Hilbert transform where the processed signal $p_r(\mathbf{r}, t)$ is the real part of the sound pressure.

In a discrete time domain, this pressure signal has a finite length and is digitally sampled, so it is represented as a finite sequence of numbers, in which the nth number in the sequence is denoted by $p_r(\mathbf{r}, n)$, where, for convenience, it is assumed $n = 0, 1, \ldots, N-1$. The discrete Hilbert transform of $p_r(\mathbf{r}, n)$ is given by [14]

$$H_d\{p_r(\mathbf{r}, n)\} = \begin{cases} \sum_{m=\text{odd}}^{N-1} \frac{p_r(\mathbf{r}, n)}{n-m} & \text{for } n \text{ even}, \\ \sum_{m=\text{even}}^{N-1} \frac{p_r(\mathbf{r}, n)}{n-m} & \text{for } n \text{ odd}, \end{cases} \tag{16}$$

therefore, the formula for calculating the pressure amplitude $P(\mathbf{r}, n)$ is as follows:

$$P(\mathbf{r}, n) = \sqrt{p_r^2(\mathbf{r}, n) + H_d^2\{p_r(\mathbf{r}, n)\}}. \tag{17}$$

It is worth noting that if we assume that $t = 0$, then Eq. (15) allows us to predict the steady-state indoor sound field for a fixed source frequency. Moreover, using Eq. (15) it is also possible to determine frequency response of a room system, defined as the frequency spectrum of the sound pressure signal received at the field point **r**, when the system is excited by a point source with a flat power spectrum.

3. Numerical study

The aim of a numerical study is to simulate the reverberant sound field in a room system consisting of two adjacent rectangular rooms of the same height. The choice of such an architectural object was dictated by the fact that a similar configuration of coupled rooms can be found in many buildings and constructions. A schematic view of this enclosure together with the associated coordinate system is shown in Fig. 1.

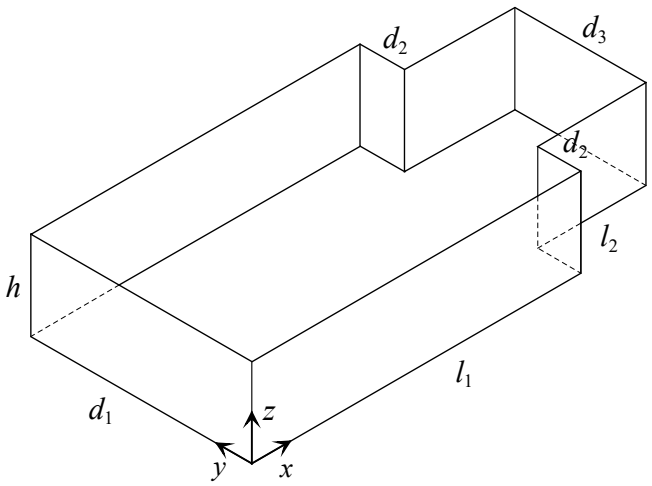

Figure 1. Room system under consideration consisting of two coupled rectangular rooms.

Numerical tests were carried out for the following dimensions of the room system: $l_1 = 15$ m, $l_2 = 5$ m, $d_1 = 10$ m, $d_2 = 2$ m, $d_3 = 6$ m and $h = 4$ m. The system was excited by the pure-tone source with the power W of 0.001 W located at the point: $\mathbf{r}_0 = (2\text{ m}, 3\text{ m}, 1.6\text{ m})$. After turning off the source, a decay of acoustic energy in the room system is the result of sound absorption on wall surfaces. If ζ_r and ζ_i are real and imaginary parts of the normalized surface impedance ζ, damping properties of this wall are described by the random-incident absorption coefficient α calculated from the formula [15]:

$$\alpha = \frac{8\zeta_r}{|\zeta|^2}\left[1 - \frac{\zeta_r \ln(1 + 2\zeta_r + |\zeta|^2)}{|\zeta|^2} + \frac{\zeta_r^2 - \zeta_i^2}{\zeta_i |\zeta|^2}\arctan\left(\frac{\zeta_i}{1+\zeta_r}\right)\right], \tag{18}$$

where $|\zeta| = \sqrt{\zeta_r^2 + \zeta_i^2}$ is a magnitude of ζ and ζ_r represents the normalized surface resistance, whereas ζ_i is referred to as the normalized surface reactance.

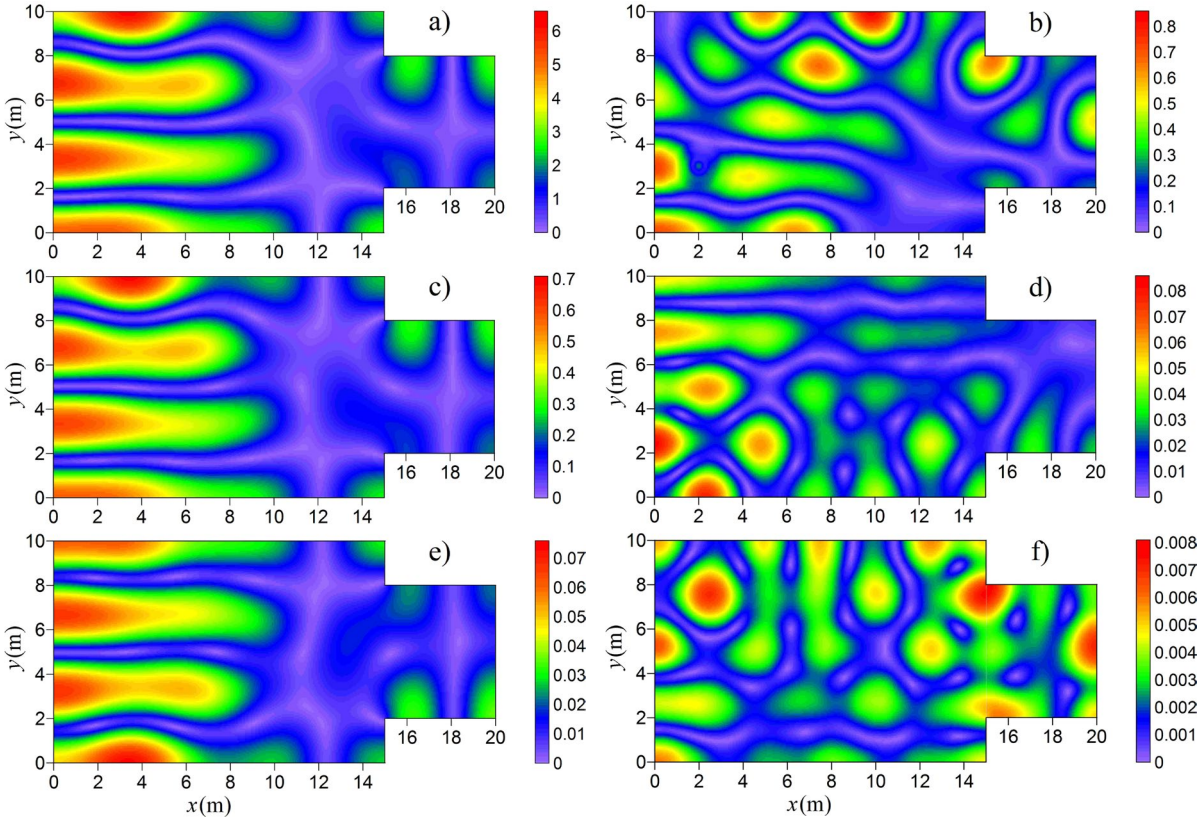

Figure 2. Distribution of the pressure amplitude P (in Pascals) on the observation plane $z = 1.2$ m for the source frequency f: (a, c, e) 52 Hz, (b, d, f) 70 Hz, and the time t: (a, b) 0 s, (c, d) 3 s, (e, f) 6 s. Hard-walled room system.

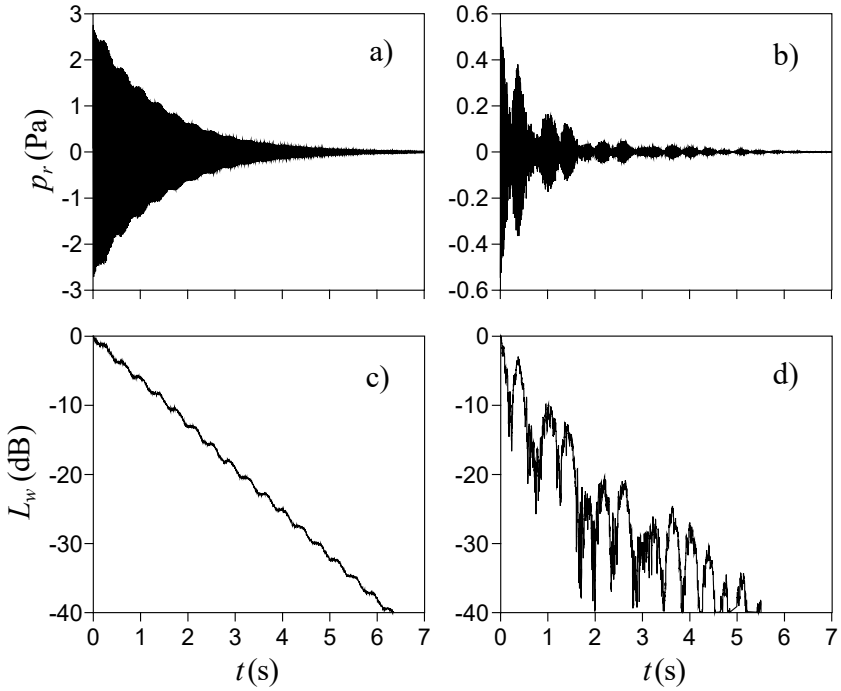

Figure 3. Temporal changes in the sound pressure p_r and the pressure level L_w at the receiver position $\mathbf{r} = (8\text{ m}, 7\text{ m}, 1.2\text{ m})$ for the source frequency f: (a, c) 52 Hz, (b, d) 70 Hz. Hard-walled room system.

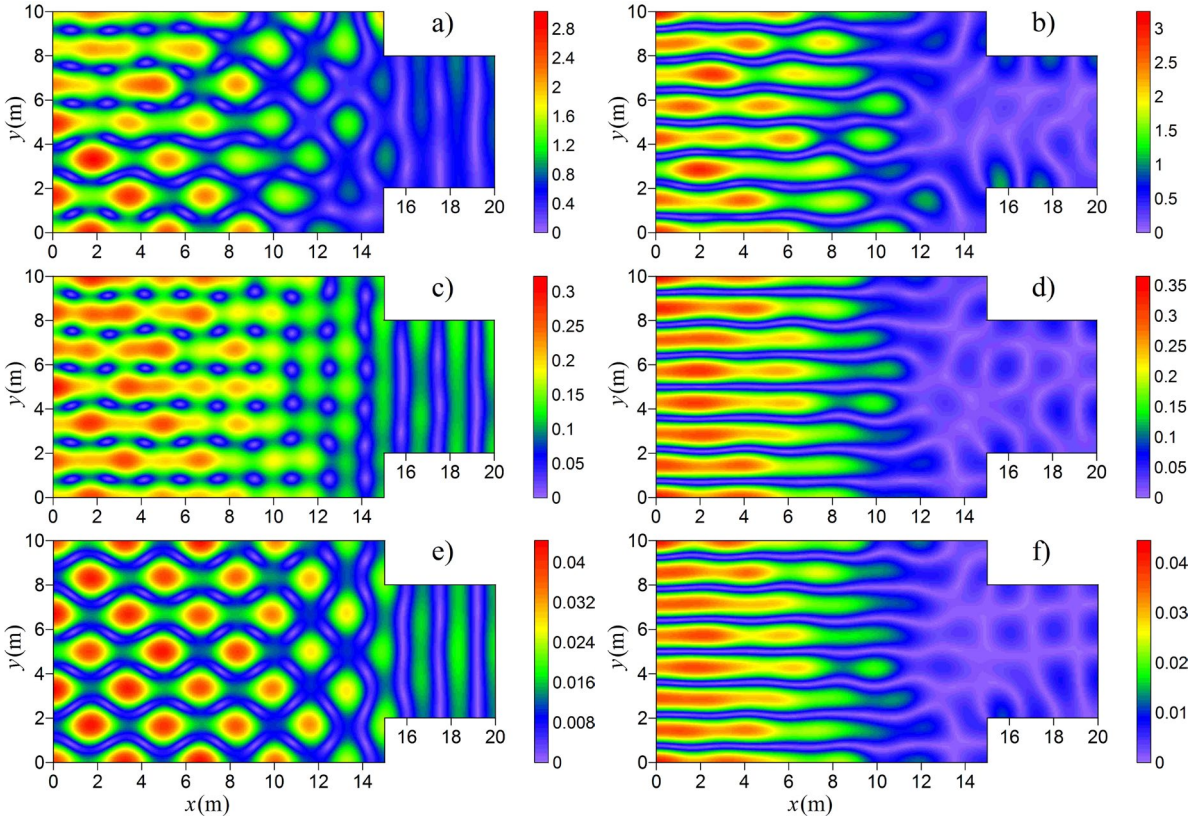

Figure 4. Distribution of the pressure amplitude P (in Pascals) on the observation plane $z = 1.2$ m for the source frequency f: (a, c, e) 103 Hz, (b, d, f) 120 Hz, and the time t: (a, b) 0 s, (c, d) 3 s, (e, f) 6 s. Hard-walled room system.

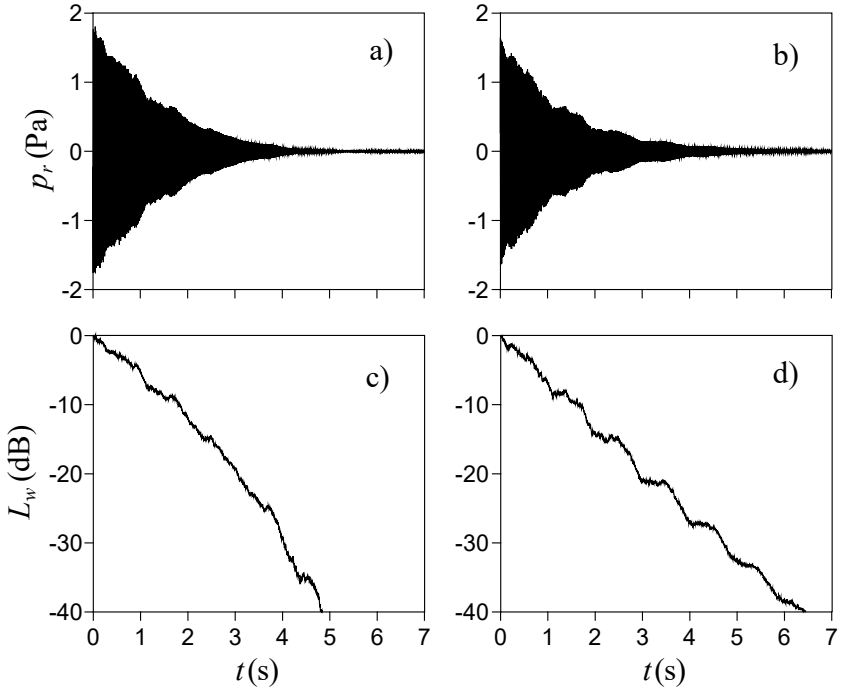

Figure 5. Temporal changes in the sound pressure p_r and the pressure level L_w at the receiver position $\mathbf{r} = (8\text{ m}, 7\text{ m}, 1.2\text{ m})$ for the source frequency f: (a, c) 103 Hz, (b, d) 120 Hz. Hard-walled room system.

As shown by Eq. (15), a computer reconstruction of the reverberant sound field requires knowledge of the eigenfunctions Φ_m. Since the considered room system has an irregular shape, analytical determination of Φ_m is not possible, so the finite element method (FEM) was employed to estimate these functions. Shapes of Φ_m were calculated for the first 800 acoustic modes and frequencies $f_m = \omega_m/2\pi$ of these modes are in the range 9.14–202.95 Hz. In the FEM procedure, a distance between adjacent nodes was 1/14 m. This means that a minimum number of nodes per wavelength is about 24, therefore in the considered frequency range this procedure demonstrates high accuracy. Numerical simulations were performed for the room system with two different absorption properties. In the first case, all walls were assumed to be hard acoustically, which means that a magnitude of the wall impedance ζ is very large but finite. In the second case, simulations were carried out for the room system after its acoustical treatment, which consisted in uniform coverage of the ceiling with a sound-absorbing material. In calculations it was assumed that an air filling the coupled rooms is characterized by the speed of sound $c = 343\,\mathrm{m/s}$ and the density $\rho = 1.21\ \mathrm{kg/m^3}$, which corresponds to a 20°C air temperature and 50% relative humidity.

An example of the hard-walled room system is an enclosure with concrete walls, thus, in numerical simulations it was assumed that walls provide uniform sound damping characterized by a real-valued surface impedance [16]. The random-incident absorption coefficient α of these walls was fixed to 0.03. In the computer algorithm the coefficient α was posited to be an input data, thus, the normalized surface resistance ζ_r of 256.15 corresponding to α equal to 0.03 was found by numerically solving the equation

$$\alpha = \frac{8}{\zeta_r}\left[1 - \frac{2\ln(1+\zeta_r)}{\zeta_r} + \frac{1}{1+\zeta_r}\right], \tag{19}$$

which can be derived from Eq. (18) by setting $\zeta_i = 0$. Numerical tests were aimed to simulate distributions of the pressure amplitude P on the observation plane $z = 1.2$ m for selected source frequencies at various times t from the moment the source was turned off ($t = 0$). Moreover, temporal changes in the sound pressure p_r and the pressure level L_w at one receiving position on the observation plane were predicted to assess the nature of sound decay at this point. The pressure level L_w was determined from the formula

$$L_w = 20\log\left(\frac{P}{P_{\max}}\right), \tag{20}$$

where $P_{\max}$ is the pressure amplitude when the sound source is switched off.

Distributions of the pressure amplitude P on the observation plane for the source frequency f (in Hz): 52, 70, 103 and 120, and the time t (in seconds): 0, 3 and 6, are shown in Figs. 2 and 4. These data indicate that it takes as much as 6 seconds after the source is turned off for the level of pressure amplitude to drop by approximately 40 dB. In the case of hard-walled room system, this is obviously due to the low sound damping on room walls. Another interesting thing resulting from these data is that for some cases the distribution of P on the observation plane does not change much over time. This effect is visible for the frequencies of 52 Hz (Fig. 2a, c, e) and 120 Hz (Fig. 4b, d, f) and is due to the fact that for these excitation frequencies there is one dominant mode in the acoustic response of the room system. As follows from Eq. (15), in such a case the sound should decay almost exponentially in time. This fact is confirmed by graphs in Figs. 3c and 5d showing temporal changes in the sound pressure p_r and pressure level L_w, simulated for the frequencies of 52 Hz and 120 Hz at the receiver point $\mathbf{r}$ = (8 m, 7 m, 1.2 m). To quantitatively assess the sound decay at this point, the reverberation time T_{30} was determined from the sound decay curves using the linear regression and its value is 9.42 s for the frequency of 52 Hz and 9.58 s for the frequency of 120 Hz. Figures 2a, c, e and 4b, d, f also prove that for the frequencies of 52 Hz and 120 Hz the acoustic energy is concentrated in a larger subroom having the dimensions $l_1 \times d_1 \times h$ (see Fig. 1). This means that for these frequencies, eigenmodes localized in this subroom are excited. In order to recognize the reason of a mode localization, the eigenfrequencies $f_{\kappa\mu\nu}$ of the hard-walled rectangular room with the same dimensions as the larger subroom were computed using the following formula [15]:

$$f_{\kappa\mu\nu} = \frac{c}{2}\sqrt{\left(\frac{\kappa}{l_1}\right)^2 + \left(\frac{\mu}{d_1}\right)^2 + \left(\frac{\nu}{h}\right)^2}, \tag{21}$$

where the modal indices κ, μ, ν are non-negative integers and they are not simultaneously equal to zero. Table 1 lists frequencies f_m of eigenmodes localized in the larger subroom and frequencies $f_{\kappa\mu\nu}$ calculated from Eq. (21) for selected modal indices κ, μ, ν. These data indicate that the effect of mode localization is caused by a generation of eigenmodes having approximately the same frequency as y-axial eigenmodes (κ, $\nu = 0$) in rectangular enclosures with the same dimensions as the larger subroom.

Table 1. Frequencies f_m of eigenmodes localized in larger subroom and frequencies $f_{\kappa\mu\nu}$ calculated from Eq. (21), together with corresponding modal indices.

m	f_m (Hz)	κ	μ	ν	$f_{\kappa\mu\nu}$ (Hz)
25	51.93	0	3	0	51.45
190	120.20	0	5	0	120.05
381	154.44	0	7	0	154.35

For the frequencies of 70 Hz and 103 Hz, large changes in distributions of the pressure amplitude P on the observation plane are noted during the sound decay process. In the first case, this is due to the fact that at the frequency of 70 Hz there is relatively weak sound excitation, as indicated by clearly smaller maximum values of P for subsequent time intervals than those observed for the frequency of 52 Hz (Fig. 2a, c, e). This means that at the frequency of 70 Hz several adjacent modes are excited and interact with each other, producing strong beating effects (Fig. 3b, d). A different behavior of sound decay occurs for the frequency of 103 Hz because excited adjacent modes have clearly different damping properties, resulting in nonlinearity of the pressure level decay curve. Generally speaking, there exist two main types of nonlinear sound decay. The convex-curved decay, as in Fig. 5c, is characterized by a slower early decay and a faster late decay, while for the concave-curved decay it is the opposite, the initial decay is faster and the late decay is slower. This fact is confirmed by the evaluation of decay times from the data in Fig. 5c, as the early decay time (EDT) and the reverberation time T_{30} predicted using the linear regression are 10.62 s and 7.31 s, thus, the EDT/T_{30} ratio becomes 1.45, which indicates a clear ballooning sound decay.

Acoustics of the hard-walled room system can be improved by placing absorbing materials on walls. However, in several situations a use of these materials on a floor or lateral walls is impossible for practical reasons, therefore in these cases the acoustical treatment is limited to a ceiling absorber. In the following, it will be assumed that the ceiling is uniformly covered with the absorbing material having the surface impedance $\zeta = 10 + \mathrm{j}5.7$, corresponding to the absorption coefficient $\alpha_c = 0.4$, and the remaining walls, as previously, are characterized by the normalized surface resistance ζ_r of 256.15 corresponding to α of 0.03. A value of α_c is appropriate to consider the room system as lightly damped, because the average absorption coefficient α_{av} for the room system after acoustical treatment of the ceiling, given by

$$\alpha_{\mathrm{av}} = \frac{\alpha(S - S_c) + \alpha_c S_c}{S}, \tag{22}$$

assumes the small value $\alpha_{\mathrm{av}} = 0.141$, where S, as before, is a surface of all room walls and S_c is a surface of the ceiling. Simulation results for the room system with ceiling treatment are depicted in Figs. 6–9. These data show that the acoustical treatment significantly reduced the reverberation because the pressure amplitude P decreases by at least 40 dB within 1.2 s of turning off the sound source. Moreover, the effect of mode localization is less noticeable due to the overlap of adjacent acoustic modes, and as a result, no exponential drop in the pressure level L_w is observed for the frequencies of localized modes (Figs. 7c, 9d).

4. Concluding remarks

In this paper, the modal expansion method was applied to determine a low-frequency reverberant sound field in coupled rooms. Theoretical study has shown that the reverberant sound that appears after turning off a pure-tone source is a superposition of decaying modal vibrations, causing the pressure amplitude to be time-dependent. Therefore, the discrete Hilbert transform was used to determine the amplitude of the decaying sound. The usefulness of the theoretical model was demonstrated in numerical tests carried out for a room system consisting of two connected rectangular rooms of the same height, because a similar configuration of coupled rooms can be found in many buildings and constructions. Eigenfunctions and eigenfrequencies of this room system were determined using the finite element method.

Calculation results obtained for the hard-walled room system showed that the source frequency has a significant impact on the distribution of pressure amplitude on the observation plane at various times after the source was turned off. This influence is the smallest for the frequencies of modes localized in one of the subrooms. This is due to the fact that at these frequencies the localized modes represent the modes that dominate the sound decay process, therefore the predicted sound decay is almost exponential. For the remaining considered source frequencies, this influence is much greater, therefore an irregular sound decay

resulting from the beating effects and a convex-curved decay characterized by a slower early decay and a faster late decay were observed.

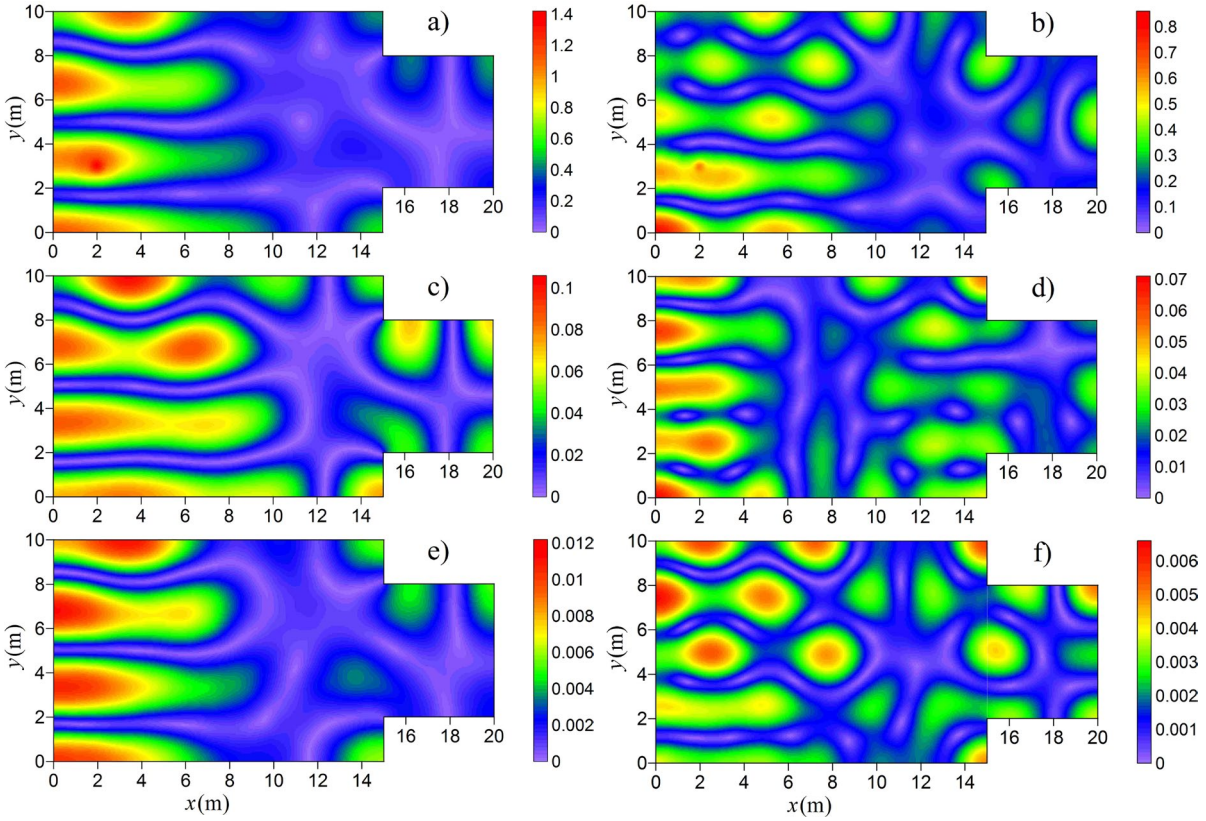

Figure 6. Distribution of the pressure amplitude P (in Pascals) on the observation plane $z = 1.2$ m for the source frequency f: (a, c, e) 52 Hz, (b, d, f) 70 Hz, and the time t: (a, b) 0 s, (c, d) 0.6 s, (e, f) 1.2 s. Room system with ceiling treatment.

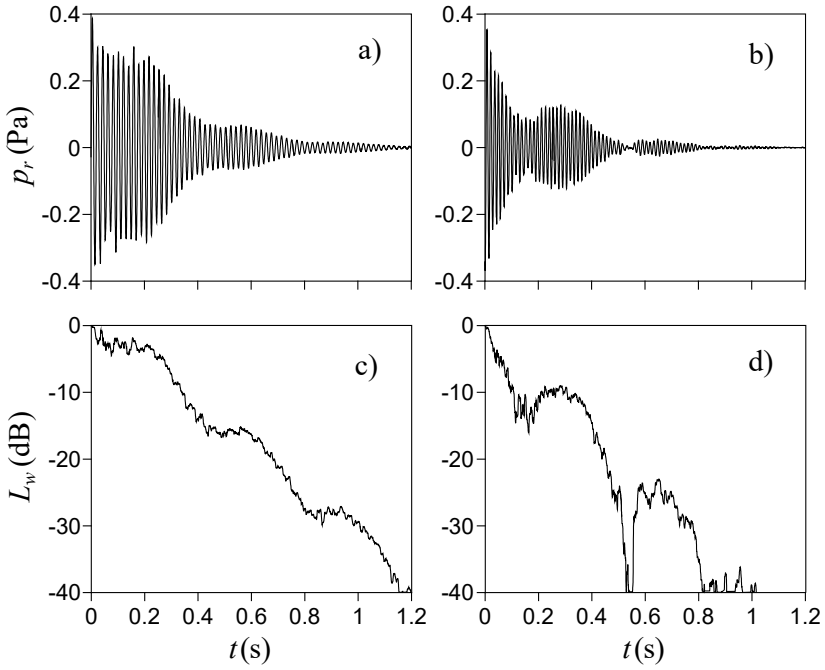

Figure 7. Temporal changes in the sound pressure p_r and the pressure level L_w at the receiver position **r =** (8 m, 7 m, 1.2 m) for the frequency f: (a, c) 52 Hz, (b, d) 70 Hz. Room system with ceiling treatment.

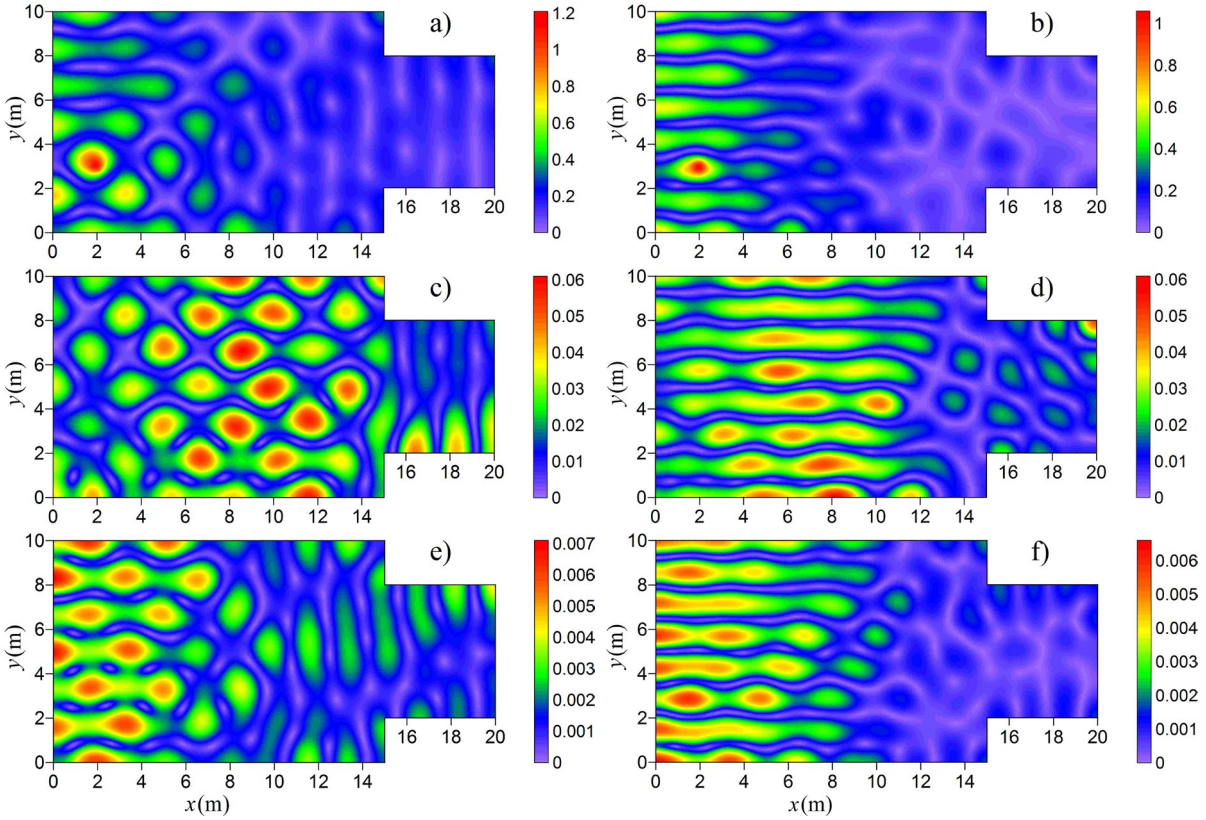

Figure 8. Distribution of the pressure amplitude P (in Pascals) on the observation plane $z = 1.2$ m for the source frequency f: (a, c, e) 103 Hz, (b, d, f) 120 Hz, and the time t: (a, b) 0 s, (c, d) 0.6 s, (e, f) 1.2 s. Room system with ceiling treatment.

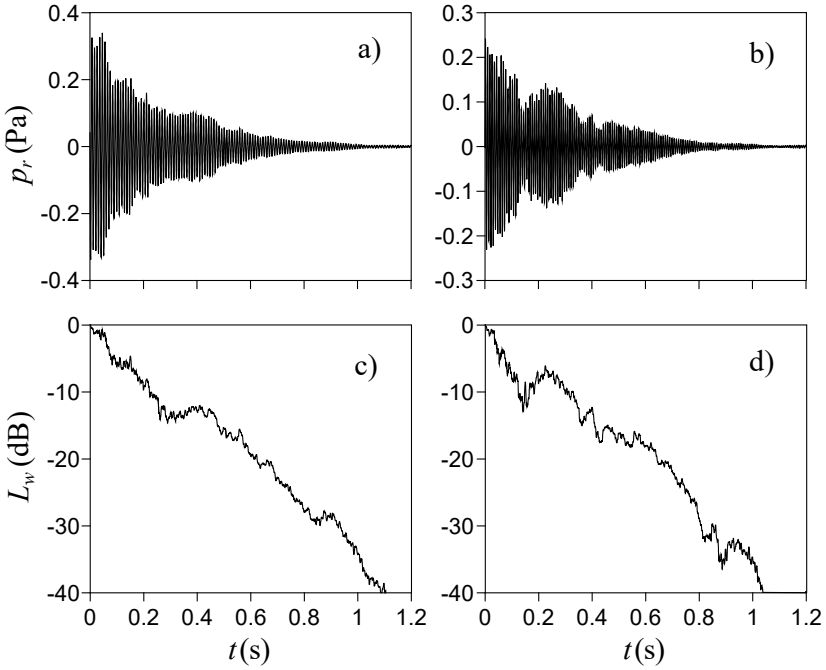

Figure 9. Temporal changes in the sound pressure p_r and the pressure level L_w at the receiver position **r =** (8 m, 7 m, 1.2 m) for the frequency f: (a, c) 103 Hz, (b, d) 120 Hz. Room system with ceiling treatment.

Numerical simulations have demonstrated that acoustical treatment of the ceiling significantly reduced reverberation. Moreover, distributions of pressure amplitude obtained in this case on the observation plane showed that for all considered frequencies the sound decay exhibits non-exponential behavior. This is due to interactions between acoustic modes that cause beating effects and the modal overlap. It can also be stated that the observed large irregularity of sound decay curves makes the proper qualification of sound decay very difficult, because in this case a characterization of the decay process by only one decay time or at most two decay times is essentially impossible.

Additional information

The author declare: no competing financial interests and that all material taken from other sources (including their own published works) is clearly cited and that appropriate permits are obtained.

References

1. N. Xiang, Y. Jing, A.C. Bockman; Investigation of acoustically coupled enclosures using a diffusion-equation model; J. Acoust. Soc. Am., 2009, 126(3), 1187–1198; DOI: 10.1121/1.3168507
2. P. Luizard, J.D. Polack, B.F.G. Katz; Sound energy decay in coupled spaces using a parametric analytical solution of a diffusion equation; J. Acoust. Soc. Am., 2014, 135(5), 2765–2776; DOI: 10.1121/1.4870706
3. J.E. Summers, R.R. Torres, Y. Shimizu; Statistical-acoustics models of energy decay in systems of coupled rooms and their relation to geometrical acoustics; J. Acoust. Soc. Am., 2004, 116(2), 958–969; DOI: 10.1121/1.1763974
4. J.E. Summers; Accounting for delay of energy transfer between coupled rooms in statistical-acoustics models of reverberant-energy decay; J. Acoust. Soc. Am., 2012, 132(2), EL129–EL134; DOI: 10.1121/1.4734591
5. L. Nijs, G. Jansens, G. Vermeir, M. van der Voorden; Absorbing surfaces in ray-tracing programs for coupled spaces; Appl. Acoust., 2002, 63(6), 611–626; DOI: 10.1016/S0003-682X(01)00063-9
6. J.E. Summers, R.R. Torres, Y. Shimizu, B.L. Dalenbäck; Adapting a randomized beam-axis-tracing algorithm to modeling of coupled rooms via late-part ray tracing; J. Acoust. Soc. Am., 2005, 118(3), 1491–1502; DOI: 10.1121/1.2000772
7. M. Meissner; K. Wiśniewski; Investigation of damping effects on low-frequency steady-state acoustical behaviour of coupled spaces; R. Soc. Open Sci., 7(8), 2020, 200514; DOI: 10.1098/rsos.200514
8. M. Meissner; Analytical and numerical study of acoustic intensity field in irregularly shaped room; Appl. Acoust., 2013, 74(5), 661–668; DOI: 10.1016/j.apacoust.2012.11.009
9. M. Meissner; Computational studies of steady-state sound field and reverberant sound decay in a system of two coupled rooms; Cent. Eur. J. Phys., 2007, 5(3), 293–312; DOI: 10.2478/s11534-007-0016-7
10. M. Meissner; Computer modelling of coupled spaces: variations of eigenmodes frequency due to a change in coupling area; Arch. Acoust., 2009, 34(2), 157–168
11. M. Meissner; Spectral characteristics and localization of modes in acoustically coupled enclosures; Acta Acustica united with Acustica, 2009, 95(2), 300–305; DOI: 10.3813/AAA.918152
12. P.J. Collins; Differential and Integral Equations; Oxford University Press, 2006
13. L. Kinsler, A. Frey, A. Coppens, J. Sander; Fundamentals of Acoustics, 4th. ed.; John Wiley & Sons, 2000
14. M. Meissner; Accuracy issues of discrete Hilbert transform in identification of instantaneous parameters of vibration signals; Acta Phys. Pol. A, 2012, 121(1A), A164–A167; DOI: 10.12693/APhysPolA.121.A-164
15. H. Kuttruff; Room Acoustics, 5th ed.; Spon Press, 2009
16. T. Thydal, F. Pind, C.H. Jeong, A.P. Engsig-Karup; Experimental validation and uncertainty quantification in wave-based computational room acoustics; Appl. Acoust., 2021, 178, 107939; DOI: 10.1016/j.apacoust.2021.107939